Acta Mech 226, 2873–2885 (2015)
DOI 10.1007/s00707-015-1361-z

ORIGINAL PAPER

XiaoChao Li · Yaoming Zhang · Yanpeng Gong · Yu Su · Xiaowei Gao

Use of the sinh transformation for evaluating 2D nearly singular integrals in 3D BEM

Received: 29 December 2014 / Revised: 19 March 2015 / Published online: 28 April 2015
© Springer-Verlag Wien 2015

Abstract This paper presents a new strategy for the numerical evaluation of 2D nearly singular integrals that arise in the solution of 3D BEM using eight-node second-order quadrilateral surface elements. The strategy is an extension of the previous sinh transformation techniques, which is used to evaluate the 1D or 2D nearly singular integrals on simple geometry elements, such as linear or planar elements. The novel feature of the proposed method is that a new distance formula is introduced here, and based on this an ingenious combination of the distance formula and the sinh transformation is developed, and hence, the rapid variation of the distance formula on the integration interval can been smoothed out. Several numerical examples involving boundary layer effect and thin-body problems in 3D potential theory are given to verify the accuracy and efficiency of the presented method.

1 Introduction

Accurate evaluation of nearly singular two-dimensional (2D) boundary element integrals has long been a challenging task to the researchers in three-dimensional (3D) boundary element method (BEM). These integrals are 'nearly' singular in the sense that the source point is close to, but not on, the element of integration. Theoretically, these integrals are regular since the values of their integrands are always finite. However, instead of remaining flat, the integrands may vary drastically on the integration interval as the evaluation point moves closer to the integration element, exhibiting similar characteristics of the singularity. The conventional Gaussian quadrature becomes inefficient or even inaccurate to evaluate these integrals. Special integration techniques are urgently required to deal with them. In this study, we focus on the numerical computation of 2D nearly singular integrals that arise in the solution of 3D BEM using eight-node second-order quadrilateral surface elements.

Tremendous effort has been devoted to derive convenient integral forms or sophisticated computational techniques for evaluating nearly singular integrals, among which the variable transformations technique, based on various nonlinear functions, seems to be a more promising approach. The methods developed so far include, but are not limited to, polynomial transformation [1,2], degenerate mapping method [3], coordinate optimal

X. Li · Y. Su
Department of Mechanics, School of Aerospace Engineering, Beijing Institute of Technology, Beijing 100081, People's Republic of China

X. Li · Y. Zhang (✉) · Y. Gong
Institute of Applied Mathematics, Shandong University of Technology, Zibo 255049, People's Republic of China
E-mail: zymfc@163.com

Y. Zhang · X. Gao
State Key Laboratory of Structural Analysis for Industrial Equipment, Dalian University of Technology, 116024 Dalian, People's Republic of China

transformation [4], sigmoidal transformation [5,6], sinh transformation [6–12], rational transformation [13], distance transformation [14–17], exponential transformation [18–23] and combinations of the polar coordinates approach and variable transformations [6]. In this work, we focus on the sinh transformation, based on the sinh function, proposed by Johnston and his collaborators [7]. The main feature of this method is to automatically take into account the position of the nearly singular point and the distance from the source point to the element. In addition, the sinh transformation techniques are applicable to a broad range of integrals without extra computational effort.

High-order geometry elements, such as the most commonly used eight-node second-order quadrilateral surface elements, are of great significance to the modeling of the complex geometrical domains, especially for thin-body structures, if sufficient accuracy is required. This is because high-order geometry elements can approximate more sufficiently boundary geometry of the domains via high-order interpolation polynomials, usually of second degree. However, it should be pointed out that the efficient estimation of nearly singular integrals over high-order geometry elements is a very difficult problem. When the geometry of the boundary element is approximated by using high-order curved surface elements, usually of the second order, the Jacobian $J(\xi_1, \xi_1)$ is not a constant but an irrational function, where ξ_1, ξ_2 are the dimensionless coordinates. The distance r between the field point and the source point is an irrational function of the type $\sqrt{p(\xi_1, \xi_2)}$, where $p(\xi_1, \xi_2)$ is the high-order polynomial. Consequently, the nearly singular integrals become more complicated and, in general, are much more difficult to solve both analytically and numerically. To date, very few studies on the calculation of nearly singular integrals over a curved surface have been reported in the BEM community [23]. Johnston and Elliott [8–10] have proposed an efficient strategy to numerically compute the nearly singular integrals over the 9-point Lagrangian curved surface element in 3D BEM using the sinh transformation, and Miao and his co-workers [12] also have done further researches on this topic. However, it is worth noting that, in their studies, only simple test integrals have been examined. In fact, to the authors' best knowledge, these methods have not, as yet, been applied to solve any practical BEM problem arising in engineering applications, although they seem to have such potential [23].

Inspired by the pioneering work mentioned above, we here extend the sinh transformation to evaluate 2D nearly singular integrals over eight-node second-order quadrilateral surface elements arising in 3D BEM. The main novel features of the proposed method lie in: (i) introducing the 'accurate' distance formula used in the exponential transformation method [23] into the sinh transformation. Such distance formula is able to accurately approximate the actual distance, r, from the evaluation point to a generic point of the element, which usually comes from the first-order Taylor expansion approximation of a curved surface element in other approaches. So promising results for numerical evaluation of 2D nearly singular integrals can be expected, (ii) an ingenious combination of the aforementioned distance formula and the sinh transformation being developed. The sinh transformation can smooth out the rapid variation of the developed distance formula on the integration interval.

The outline of the rest of this paper is as follows. The general form of nearly singular integrals is described in Sect. 2. Then, in Sect. 3, the distance function, based on the eight-node second-order quadrilateral surface elements, is constructed. Section 4 considers the regularization of nearly singular integrals over high-order geometrical elements using the sinh transformation. In Sect. 5, the accuracy and stability of the proposed scheme are tested on three 3D potential examples with known benchmark solutions. Finally, the conclusions are provided in Sect. 6.

2 General descriptions

In this paper, we always assume that Ω is a bounded domain in R^3, Ω^c is its open complement, and Γ denotes the common boundary. $\boldsymbol{n}(\boldsymbol{x})$ is the unit outward normal vector on Γ to the domain Ω at the point $\boldsymbol{x}$. By omitting the body sources in potential problems, the regularized BIEs with indirect unknowns on $\hat{\Omega}$ can be expressed as

$$\begin{aligned} u(\boldsymbol{y}) &= \int_{\Gamma} \phi(\boldsymbol{x}) u^*(\boldsymbol{x}, \boldsymbol{y}) d\Gamma_{\boldsymbol{x}}, \ \ \boldsymbol{y} \in \hat{\Omega}, \\ \frac{\partial u(\boldsymbol{y})}{\partial \hat{\boldsymbol{n}}(\boldsymbol{y})} &= \hat{S}\phi(\boldsymbol{y}) + \int_{\Gamma} [\phi(\boldsymbol{x}) - \phi(\boldsymbol{y})] \frac{\partial u^*(\boldsymbol{x}, \boldsymbol{y})}{\partial \hat{\boldsymbol{n}}(\boldsymbol{y})} \mathrm{d}\Gamma + \phi(\boldsymbol{y}) \int_{\Gamma} \left[\frac{\partial u^*(\boldsymbol{x}, \boldsymbol{y})}{\partial \hat{\boldsymbol{n}}(\boldsymbol{y})} + \frac{\partial u^*(\boldsymbol{x}, \boldsymbol{y})}{\partial \hat{\boldsymbol{n}}(\boldsymbol{x})} \right] \mathrm{d}\Gamma, \quad \boldsymbol{y} \in \Gamma. \end{aligned} \tag{1}$$

For the internal point $\boldsymbol{y}$ the integral equations can be written as

$$\begin{aligned} u(\boldsymbol{y}) &= \int_{\Gamma} \phi(\boldsymbol{x}) u^*(\boldsymbol{x}, \boldsymbol{y}) \mathrm{d}\Gamma_{\boldsymbol{x}}, \ \boldsymbol{y} \in \hat{\Omega}, \\ \nabla_{\boldsymbol{y}} u(\boldsymbol{y}) &= \int_{\Gamma} \phi(\boldsymbol{x}) \nabla_{\boldsymbol{y}} u^*(\boldsymbol{x}, \boldsymbol{y}) \mathrm{d}\Gamma_{\boldsymbol{x}}, \ \boldsymbol{y} \in \hat{\Omega}. \end{aligned} \tag{2}$$

In Eqs. (1–2), $\phi(\boldsymbol{x})$is the density function to be determined; $u^*(\boldsymbol{x}, \boldsymbol{y})$ denotes the Kelvin fundamental solution. For interior problems, $\hat{\Omega} = \Omega$, $\hat{S} = 1$, $\hat{\boldsymbol{n}}(\boldsymbol{x})$ is the unit outward normal vector on Γ to domain Ω at point x. For exterior problems, $\hat{\Omega} = \Omega^c$, $\hat{S} = 0$, $\hat{\boldsymbol{n}}(\boldsymbol{x})$ is the unit outward normal vector on Γ to domain Ω^c at point x.

For the discretized form of Eq. (2), when the field point $\boldsymbol{y}$ is far enough from the integration elements, a straightforward application of Gaussian quadrature procedure suffices to evaluate such integrals. However, when the field point $\boldsymbol{y}$ is very close to the integration elements Γ_e, the distance r between the field point $\boldsymbol{y}$ and the source point x is almost zero. Hence, the integrals in the discretized Eq. (2) are nearly singular and the numerical integrations by the standard Gaussian quadrature fail. These nearly singular integrals can be expressed as

$$\mathrm{I} = \int_{\Gamma_e} \frac{f(x, y)}{r^{\alpha}} \mathrm{d}\Gamma \tag{3}$$

where $r = \|\boldsymbol{x} - \boldsymbol{y}\|_2$, $\alpha > 0$ is a real constant, and $f(x, y)$ denotes a well-behaved function.

3 Nearly singular integrals on paraboloidal surface elements

In this paper, the geometry segment is modeled by a continuous paraboloidal element, which has eight knots; namely, the boundary geometry is approximated by the piecewise continuous eight-node second-order quadrilateral surface elements, while the distribution of the boundary quantities over each of these segments is approximated using discontinuous elements, eight nodes of which are located away from the edges of the element.

Assume $\boldsymbol{x}^j = (x_1^j, x_2^j, x_3^j)$, $j = 1, \ldots, 8$ are the eight knots of the segment Γ_j, then Cartesian coordinates of the points on the element Γ_j can be interpolated as

$$x_k(\xi_1, \xi_2) = \sum_{j=1}^{8} N_j(\xi_1, \xi_2) x_k^j, \quad k = 1, 2, 3 \tag{4}$$

where

$$\begin{aligned} &N_1(\xi_1, \xi_2) = \frac{1}{4}(1 - \xi_1)(1 - \xi_2)(-\xi_1 - \xi_2 - 1), \quad N_2(\xi_1, \xi_2) = \frac{1}{4}(1 + \xi_1)(1 - \xi_2)(\xi_1 - \xi_2 - 1), \\ &N_3(\xi_1, \xi_2) = \frac{1}{4}(1 + \xi_1)(1 + \xi_2)(\xi_1 + \xi_2 - 1), \quad N_4(\xi_1, \xi_2) = \frac{1}{4}(1 - \xi_1)(1 + \xi_2)(-\xi_1 + \xi_2 - 1), \\ &N_5(\xi_1, \xi_2) = \frac{1}{2}(1 - \xi_1^2)(1 - \xi_2), \quad N_6(\xi_1, \xi_2) = \frac{1}{2}(1 + \xi_1)(1 - \xi_2^2), \\ &N_7(\xi_1, \xi_2) = \frac{1}{2}(1 + \xi_2)(1 - \xi_1^2), \quad N_8(\xi_1, \xi_2) = \frac{1}{2}(1 - \xi_1)(1 - \xi_2^2), \quad -1 \le \xi_1 \le 1, \quad -1 \le \xi_2 \le 1. \end{aligned} \tag{5}$$

3.1 Determination of the projection point

The minimum distance d from the field point $\boldsymbol{y}$ to the integration element Γ_e is defined as the length $|\boldsymbol{y} - \boldsymbol{x}^p|$, where $\boldsymbol{x}^p$ is the projection point of $\boldsymbol{y}$ onto the integration element Γ_e. Letting $(\eta_1, \ \eta_2)$ be the local coordinates of the projection point $\boldsymbol{x}^p$, i.e., $\boldsymbol{x}^p = (x_1(\eta_1, \eta_2), x_2(\eta_1, \eta_2), x_3(\eta_1, \eta_2))$, then $\eta_1, \ \eta_2$ are the real roots of the following equation:

$$\begin{cases} [x_i(\eta_1, \eta_2) - y_i] \frac{\partial x_i}{\partial \xi_1} = 0 \\ [x_i(\eta_1, \eta_2) - y_i] \frac{\partial x_i}{\partial \xi_2} = 0 \end{cases}, \quad i = 1, 2, 3 \tag{6}$$

in which the summation convention is used, and $\frac{\partial x_i}{\partial \xi_k} = \frac{\partial x_i}{\partial \xi_k}\Big|_{\substack{\xi_1=\eta_1\\ \xi_2=\eta_2}}$, $k = 1, 2$. These assumptions will be applied also in what follows unless specified otherwise.

If the source point $\boldsymbol{y}$ is sufficiently close to the boundary Γ, then $\boldsymbol{x^p}$ is inside the integration element, and Eq. (6) has a pair of the unique real roots $(\eta_1,\ \eta_2) \in [-1, 1] \times [-1, 1]$. The real roots $\eta_1,\ \eta_2$ can be evaluated numerically by using the Newton's method. Setting

$$f_1(\eta_1, \eta_2) = [x_i(\eta_1, \eta_2) - y_i]\frac{\partial x_i}{\partial \xi_1}, \quad f_2(\eta_1, \eta_2) = [x_i(\eta_1, \eta_2) - y_i]\frac{\partial x_i}{\partial \xi_2},$$

the formula of the Newton's method can be expressed as

$$F'(\boldsymbol{\eta}^{(k)})\Delta\boldsymbol{\eta}^{(k)} = -F(\boldsymbol{\eta}^{(k)}) \tag{7}$$

where

$$\Delta\boldsymbol{\eta}^{(k)} = \boldsymbol{\eta}^{(k+1)} - \boldsymbol{\eta}^{(k)}, \quad \boldsymbol{\eta}^{(k)} = \left(\eta_1^{(k)}, \eta_2^{(k)}\right)^{\mathrm{T}}, \quad \boldsymbol{\eta}^{(k+1)} = \left(\eta_1^{(k+1)}, \eta_2^{(k+1)}\right)^{\mathrm{T}},$$
$$F(\boldsymbol{\eta}^{(k)}) = \begin{bmatrix} f_1(\eta_1^{(k)}, \eta_2^{(k)}) \\ f_2(\eta_1^{(k)}, \eta_2^{(k)}) \end{bmatrix}, \quad F'(\boldsymbol{\eta}^{(k)}) = \begin{bmatrix} \frac{\partial f_1}{\partial \eta_1} & \frac{\partial f_1}{\partial \eta_2} \\ \frac{\partial f_2}{\partial \eta_1} & \frac{\partial f_2}{\partial \eta_2} \end{bmatrix}_{\boldsymbol{\eta}=\boldsymbol{\eta}^{(k)}};$$

here

$$\frac{\partial f_j}{\partial \eta_m} = \sum_i^3 \left(\frac{\partial x_i}{\partial \xi_m}\frac{\partial x_i}{\partial \xi_j} + [x_i(\eta_1, \eta_2) - y_i]\frac{\partial^2 x_i}{\partial \xi_j \partial \xi_m}\right), \quad j, m = 1, 2.$$

3.2 Form of distance function r^2

$x_k(\xi_1, \xi_2)$ can be expressed as

$$\begin{aligned} x_k(\xi_1, \xi_2) = x_k(\eta_1, \eta_2) &+ (\xi_1 - \eta_1)\frac{\partial x_k}{\partial \xi_1} + (\xi_2 - \eta_2)\frac{\partial x_k}{\partial \xi_2} \\ &+ \frac{1}{2}\left[(\xi_1 - \eta_1)^2\frac{\partial^2 x_k}{\partial \xi_1^2} + 2(\xi_1 - \eta_1)(\xi_2 - \eta_2)\frac{\partial^2 x_k}{\partial \xi_1 \partial \xi_2} + (\xi_2 - \eta_2)^2\frac{\partial^2 x_k}{\partial \xi_2^2}\right]. \end{aligned} \tag{8}$$

Using Eq. (8), the distance square r^2 between the source point $\boldsymbol{y}$ and the field point $\boldsymbol{x}(\xi_1, \xi_2)$ can be written as

$$\begin{aligned} r^2(\xi_1, \xi_2) &= [x_k(\xi_1, \xi_2) - y_k]\,[x_k(\xi_1, \xi_2) - y_k] \\ &= d^2 + (\xi_\alpha - \eta_\alpha)\tilde{g}_\alpha + (\xi_\alpha - \eta_\alpha)(\xi_\beta - \eta_\beta)\tilde{g}_{\alpha\beta} \\ &\quad + (\xi_\alpha - \eta_\alpha)(\xi_\beta - \eta_\beta)(\xi_\gamma - \eta_\gamma)\tilde{g}_{\alpha\beta\gamma} \\ &\quad + (\xi_\alpha - \eta_\alpha)(\xi_\beta - \eta_\beta)(\xi_\gamma - \eta_\gamma)(\xi_\mu - \eta_\mu)\tilde{g}_{\alpha\beta\gamma\mu} \end{aligned} \tag{9}$$

where the summation rule is applied with respect to the Latin indices (taken from the range 1, 2, 3) and Greek indices (taken from the range 1, 2),

$$\begin{aligned} d^2 &= \left(y_k - x_k^p\right)\left(y_k - x_k^p\right), \\ \tilde{g}_\alpha &= 2\left(y_k - x_k^p\right)x_{k,\alpha},\ x_{k,\alpha} = \frac{\partial x_k}{\partial \xi_\alpha}\Big|_{\substack{\xi_1=\eta_1\\ \xi_2=\eta_2}}, \\ \tilde{g}_{\alpha\beta} &= \left(y_k - x_k^p\right)x_{k,\alpha\beta} + x_{k,\alpha}x_{k,\beta} = \tilde{g}_{\beta\alpha}, \\ \tilde{g}_{\alpha\beta\gamma} &= x_{k,\alpha\beta}x_{k,\gamma} = \tilde{g}_{\beta\alpha\gamma},\ \tilde{g}_{\alpha\beta\gamma\mu} = \frac{1}{4}x_{k,\alpha\beta}x_{k,\gamma\mu} = \tilde{g}_{\beta\alpha\gamma\mu}. \end{aligned}$$

Recall that $\tilde{g}_\alpha \equiv 0$, since $(y_k - x_k^p)$ is orthogonal to the element and $x_{k,\alpha}$ is tangential to the element at the projection point $\boldsymbol{x}^p$. Thus, Eq. (10) can be rewritten as

$$\begin{aligned} r^2(\xi_1, \xi_2) &= d^2 + (\xi_\alpha - \eta_\alpha)(\xi_\beta - \eta_\beta)\hat{g}_{\alpha\beta} \\ &= d^2 + (\xi_1 - \eta_1)^2 g_{11} + (\xi_2 - \eta_2)^2 g_{22} + (\xi_1 - \eta_1)(\xi_2 - \eta_2) g_{12} \end{aligned} \tag{10}$$

where

$$\begin{aligned} &\hat{g}_{\alpha\beta} = \tilde{g}_{\alpha\beta} + (\xi_\gamma - \eta_\gamma)\tilde{g}_{\alpha\beta\gamma} + (\xi_\gamma - \eta_\gamma)(\xi_\mu - \eta_\mu)\tilde{g}_{\alpha\beta\gamma\mu}, \\ &g_{11} = \hat{g}_{11}, \quad g_{22} = \hat{g}_{22}, \quad g_{12} = \hat{g}_{12} + \hat{g}_{21} = 2\hat{g}_{12}. \end{aligned}$$

3.3 Nearly singular integrals on the second-order elements

By some simple deductions and based on the expression form (10) of the distance function r^2, the nearly singular integrals in Eq. (3) would be reduced to the following form:

$$\mathrm{I} = \int_0^B \int_0^A \frac{f(x, y)}{\left[d^2 + x^2 g_{11}(x, y) + y^2 g_{22}(x, y) + xy g_{12}(x, y)\right]^\alpha} \mathrm{d}x\mathrm{d}y \tag{11}$$

where A, B are two constants which are possibly different values in different integrals; $f(\cdot)$ is a regular function that consists of shape functions, Jacobian and terms which arise from taking the derivative of the integral kernels.

4 Variable transformation

In this section, the proposed sinh transformation is extended to dealing with the two-dimensional nearly singular integrals over paraboloidal surface elements in the three-dimensional boundary element method. The proposed transformation can be expressed as follows:

$$x = d\sinh(m_1 + m_2 s), \quad y = d\sinh(n_1 + n_2 t), \quad -1 \le s \le 1, \quad -1 \le t \le 1 \tag{12}$$

where $m_1 = m_2 = \operatorname{arcsinh}(A/d)/2, n_1 = n_2 = \operatorname{arcsinh}(B/d)/2$.

The Jacobian of transformation (12) is then given by

$$|J| = d^2 m_2 n_2 \cosh(m_1 + m_2 s)\cosh(n_1 + n_2 t). \tag{13}$$

Substituting (12) into Eq. (11), we obtain the following equation:

$$\mathrm{I} = \frac{1}{d^{2\alpha-2}} \int_{-1}^{1} \int_{-1}^{1} \frac{f(s, t) m_2 n_2 \cosh(m_1 + m_2 s)\cosh(n_1 + n_2 t)}{F(s, t)} \mathrm{d}s\mathrm{d}t \tag{14}$$

where

$$\begin{aligned} F(s, t) = [1 &+ \sinh^2(m_1 + m_2 s) g_{11}(s, t) + \sinh^2(n_1 + n_2 t) g_{22}(s, t) \\ &+ \sinh(m_1 + m_2 s)\sinh(n_1 + n_2 t) g_{12}(s, t)]^\alpha . \end{aligned}$$

By following the procedures described above, the nearly singularity of the boundary integrals has been fully regularized. The final integral formulations over curved boundary elements are obtained as shown in Eq. (14), which can be computed straightforward by using standard Gaussian quadrature.

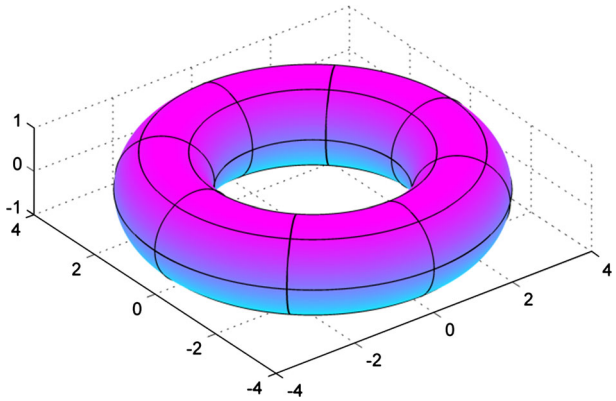

Fig. 1 Discretization of the torus with 80 second-order surface elements

5 Numerical examples

In order to verify the effectiveness of the proposed technique, three numerical examples of 3D potential problems are investigated below. The geometry boundary is depicted by eight-node second-order quadrilateral surface elements, and the boundary functions are approximated by the same type of discontinuous interpolation functions. The eighteen-point standard Gaussian integration is used for the calculation of the various element integrals unless specified otherwise. For the nearly singular integrals the standard Gaussian quadrature is employed after application of the proposed transformation. The results obtained by using the present method as well as by the conventional algorithm (without any transformation) and the exact solutions are all presented for convenience of comparison, in order to demonstrate the usefulness of the proposed method.

The numerical solution accuracy at a single computed point is assessed by means of the relative error defined by

$$\mathrm{RE} = \left| \frac{I_{\mathrm{exa}} - I_{\mathrm{num}}}{I_{\mathrm{exa}}} \right|$$

where I_{num} and I_{exa} denote the numerical and exact values at the evaluation points, respectively. Furthermore, the average relative error (*ARE*) of the multiple computational results is defined by

$$\mathrm{ARE} = \sqrt{\sum_{k=1}^{M} \left(I_{\mathrm{num}}^{k} - I_{\mathrm{exa}}^{k}\right)^2 / \sum_{k=1}^{M} \left|I_{\mathrm{exa}}^{k}\right|^2}$$

where M is the number of the interior evaluation points.

In what follows, d denotes the distance between the evaluation point and the integration boundary element.

Example 1 As shown in Fig. 1, this example concerns a problem in a torus centered at origin, with the exterior radius and interior radius being $R = 3$ and $r = 1$, respectively. The parametric equation of the boundary surface is

$$x_1 = (R + r\cos\theta)\cos\varphi, \quad x_2 = (R + r\cos\theta)\sin\varphi, \quad x_3 = r\sin\theta, \ 0 \le \theta \le 2\pi, \quad 0 \le \varphi \le 2\pi.$$

The prescribed potential distribution on the boundary is

$$u = x_1^2 - x_3^2 + x_1x_2 + x_2x_3 - 2x_1 + 1.$$

The boundary surface of the torus is discretized by 80 second-order quadrilateral surface elements. The numerical solutions for the potentials u and the fluxes $\partial u/\partial x_1$ at internal points along the x_1-axis are listed in Tables 1 and 2, respectively. Hence, we can observe that when the evaluation points are not too close to the boundary, both the methods with and without transformation of the integration variables are effective and can give acceptable results. As the evaluation point approaches the boundary element of integration, i.e., when the distance of the internal point from the integration element is equal to or less than 0.01, the results of the conventional method become less satisfactory. On the other hand, the results of the proposed method are still

Table 1 Potentials u at internal points increasingly close to the boundary

Interior points	Exact	No transform	Present	
			Numerical	Relative error
(2. 0001,0,0)	1.007666	1.128092	1.003588	4.046417E–03
(2. 001,0,0)	1.009474	1.128620	1.005400	4.035724E–03
(2. 01,0,0)	1.027640	1.136976	1.023604	3.926795E–03
(2. 1,0,0)	1.218210	1.209839	1.214820	2.782792E–03
(2.2,0,0)	1.440000	1.430107	1.437461	1.763063E–03
(2.6,0,0)	2.560000	2.560376	2.559541	1.794608E–03
(3.0,0,0)	4.000000	4.000731	4.000438	1.094613E–03
(3.4,0,0)	5.760000	5.726179	5.755770	7.344121E–03
(3.8,0,0)	7.840000	7.801368	7.833435	8.373920E–03
(3.9,0,0)	8.410000	8.558704	8.404022	7.108219E–03
(3.99,0,0)	8.940100	12.121401	8.935828	4.778300E–03
(3.999,0,0)	8.976016	12.157652	8.971904	4.581146E–03

Table 2 Fluxes $\partial u/\partial x_1$ at internal points increasingly close to the boundary

Interior points	Exact	No transform	Present	
			Numerical	Relative error
(2.0001,0,0)	2.007651	0.553920	2.011478	1.906012E–03
(2.001,0,0)	2.009451	0.618515	2.013358	1.944084E–03
(2.01,0,0)	2.027451	1.218043	2.032116	2.300681E–03
(2.1,0,0)	2.207451	2.203175	2.208647	3.930504E–03
(2.2,0,0)	2.400000	2.401970	2.408492	3.538399E–03
(2.6,0,0)	3.200000	3.200439	3.202832	8.850165E–03
(3.0,0,0)	4.000000	4.001484	4.000438	1.094613E–03
(3.4,0,0)	4.800000	4.803833	4.793360	1.383321E–03
(3.8,0,0)	5.600000	5.612679	5.600656	1.170607E–03
(3.9,0,0)	5.800000	5.695471	5.812065	2.080162E–03
(3.99,0,0)	5.980000	0.835980	6.006151	4.373007E–03
(3.999,0,0)	5.992000	0.954581	5.992000	4.525456E–03

steady and satisfactory even when the interior points are very close to the boundary. This can be seen from the relative errors with respect to the exact solutions which are also shown in Tables 1 and 2 and demonstrate the efficiency and the usefulness of the developed algorithm.

Furthermore, on the inner surface

$$\mathrm{S}_1{:}x_1 = (3 + 0.99\cos\theta)\cos\varphi, \quad x_2 = (3 + 0.99\cos\theta)\sin\varphi, \quad x_3 = 0.99\sin\theta,$$
$$0 \le \theta \le 2\pi, \quad 0 \le \varphi \le 2\pi,$$

320 interior points, uniformly spaced with respect to θ and ϕ, are taken into account. Figure 2a, b displays the profiles of the analytical solutions for the potentials u and fluxes $\partial u/\partial x_1$ on the inner spherical surface S_1, respectively, and Fig. 3a, b shows the surfaces of the numerical solutions for the potentials u and its derivatives $\partial u/\partial x_1$ at these 320 interior points, respectively. Hence, we can see from the comparison of Figs. 2a, b and 3a, b that the numerical results match the exact solution very well. Figure 4a, b shows the relative error surfaces of the computational results for the potentials u and fluxes $\partial u/\partial x_1$ at these 320 interior points, where their AREs are 7.6206×10^{-4} and 5.1547×10^{-3} at these 320 interior points, respectively. Hence, it can be seen that the proposed method is accurate.

Example 2 As shown in Fig. 5, a mixed boundary-value problem in a cylindrical tube Ω centered at $(0, 0, 0)$ is considered in this example, such that

$$\Omega = \left\{ (x_1, x_2, x_3) \in R^3 : 2 < \sqrt{x_1^2 + x_2^2} < 4, -5 < x_3 < 5 \right\}.$$

On the boundary Γ, the potential u is prescribed on the top face $\left\{ 2 \le \sqrt{x_1^2 + x_2^2} \le 4, x_3 = 5 \right\}$, and the flux $q = \boldsymbol{n} \cdot \nabla u$ is given on the remaining surface components of Γ, where

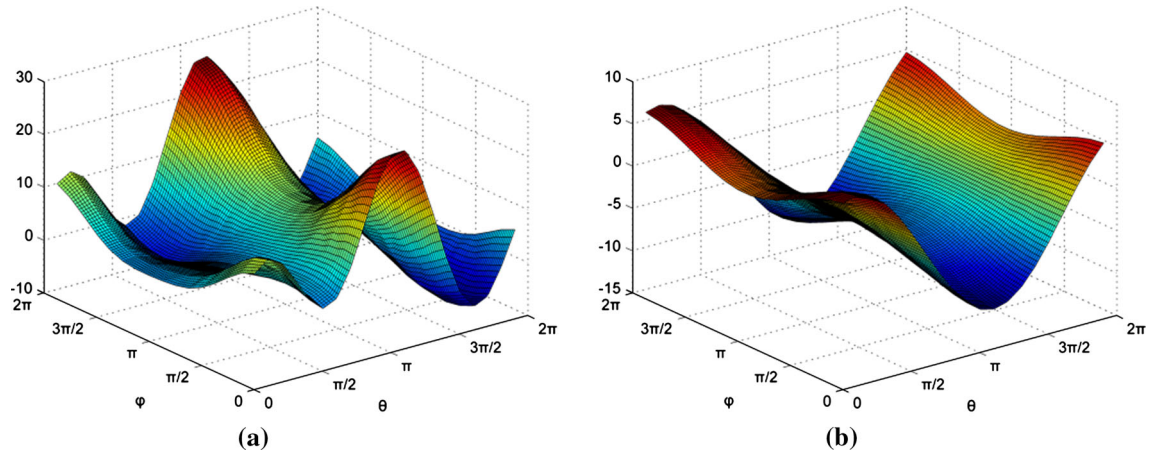

Fig. 2 Profiles of the analytical solutions for the potentials (**a**) and its derivatives (**b**)

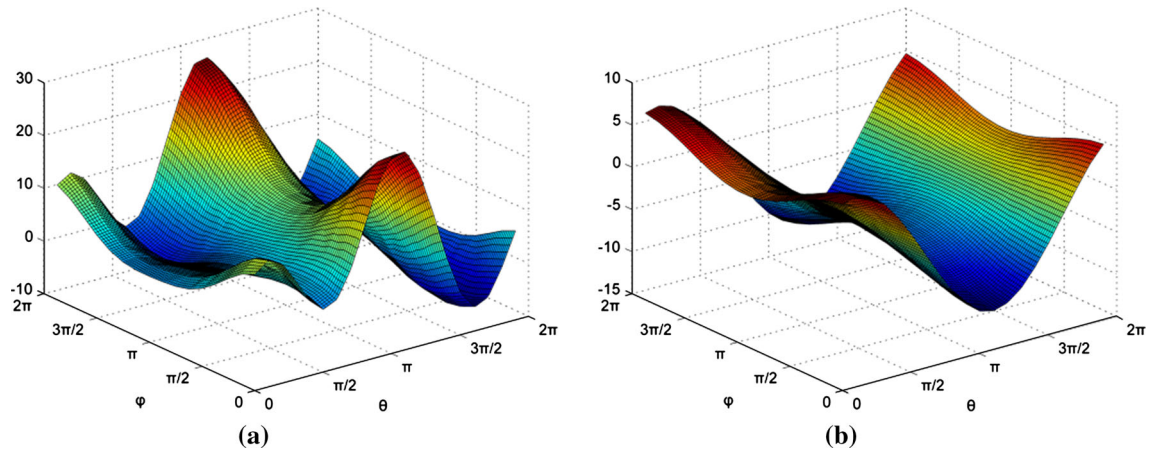

Fig. 3 Profiles of the numerical solutions for the potentials (**a**) and its derivatives (**b**)

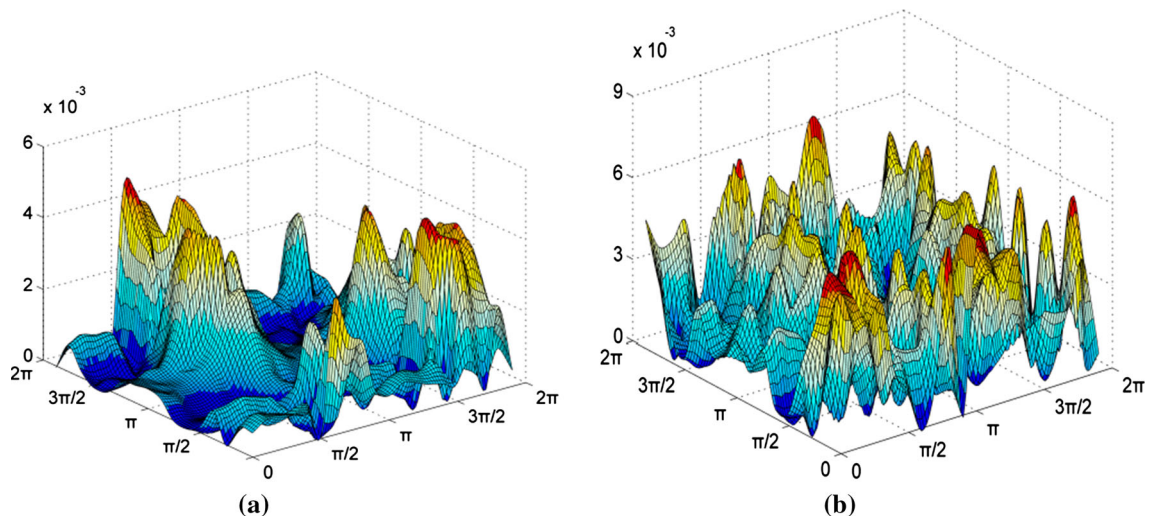

Fig. 4 Surfaces of REs for the potentials (**a**) and its derivatives (**b**) with eighty discretization boundary elements

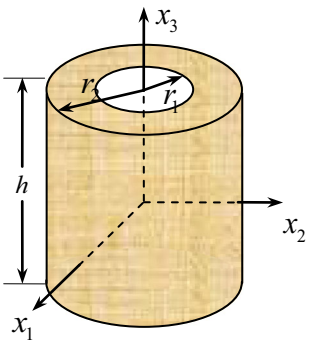

Fig. 5 A mixed boundary-value problem in a cylindrical tube

Table 3 Potentials u at internal points increasingly close to the outer boundary

Distance d	Exact	No transform	Present	
			Numerical	Relative error
0.1	0.5931900E+02	0.5927756E+02	0.5929656E+02	3.783496E−04
0.01	0.6352120E+02	0.6227269E+02	0.6349058E+02	4.820358E−04
0.001	0.6395201E+02	0.6225023E+02	0.6392043E+02	4.938404E−04
0.0001	0.6399520E+02	0.6224245E+02	0.6396352E+02	4.950364E−04
0.00001	0.6399952E+02	0.6224161E+02	0.6396783E+02	4.951579E−04
0.000001	0.6399995E+02	0.6224153E+02	0.6396826E+02	4.951775E−04
0.0000001	0.6400000E+02	0.6224152E+02	0.6396830E+02	4.951890E−04
0.00000001	0.6400000E+02	0.6224152E+02	0.6396831E+02	4.951747E−04
0.000000001	0.6400000E+02	0.6224152E+02	0.6396832E+02	4.950759E−04
0.0000000001	0.6400000E+02	0.6224152E+02	0.6396833E+02	4.948031E−04

Table 4 Potential derivatives $\partial u/\partial x_1$ at internal points increasingly close to the outer boundary

Distance d	Exact	No transform	Present	
			Numerical	Relative error
0.1	0.4563000E+02	0.4458462E+02	0.4555244E+02	1.699758E−03
0.01	0.4776030E+02	0.3018469E+01	0.4765494E+02	2. 206029E−03
0.001	0.4797600E+02	−0.8086343E+01	0.4786744E+02	2.262867E−03
0.0001	0.4799760E+02	−0.9213227E+01	0.4788871E+02	2.268619E−03
0.00001	0.4799976E+02	−0.9325899E+01	0.4789084E+02	2.269241E−03
0.000001	0.4799998E+02	−0.9337166E+01	0.4789104E+02	2.269487E−03
0.0000001	0.4800000E+02	−0.9338293E+01	0.4789105E+02	2.269826E−03
0.00000001	0.4800000E+02	−0.9338405E+01	0.4789104E+02	2.270017E−03
0.000000001	0.4800000E+02	−0.9338417E+01	0.4789108E+02	2.269247E−03
0.0000000001	0.4800000E+02	−0.9338418E+01	0.4789123E+02	2.266044E−03

$$u = x_1^3 + 2x_2^3 + 3x_3^3 - 3x_1x_3^2 - 6x_2x_1^2 - 9x_3x_2^2,$$
$$\nabla u = (3x_1^2 - 3x_3^2 - 12x_1x_2, -6x_1^2 + 6x_2^2 - 18x_2x_3, -9x_2^2 + 9x_3^2 - 6x_1x_3).$$

To solve the problem numerically, the boundary Γ is totally divided by 98 quadrilateral surface elements, where 50 elements are on the outer side face, 32 elements on the inner side face, 8 elements on the top face and 8 elements on the bottom face, respectively. The numerical solutions for the potentials u and its derivatives $\partial u/\partial x_1$ (in the x_1 direction) at internal points are listed in Tables 3 and 4, respectively; hence, we can see that when the evaluation points are not too close to the boundary, both the methods with and without transformation of the integration variables are effective and can give acceptable results. As the evaluation point approaches the boundary element of integration, i.e., when the distance of the internal point from the integration element is equal to or less than 0.001, the results of the conventional method become less satisfactory. On the other hand, the results of the proposed method are still steady and satisfactory even when the distance of the evaluation point to the integration element reaches 1E−10. This can be seen from the relative errors with respect to the

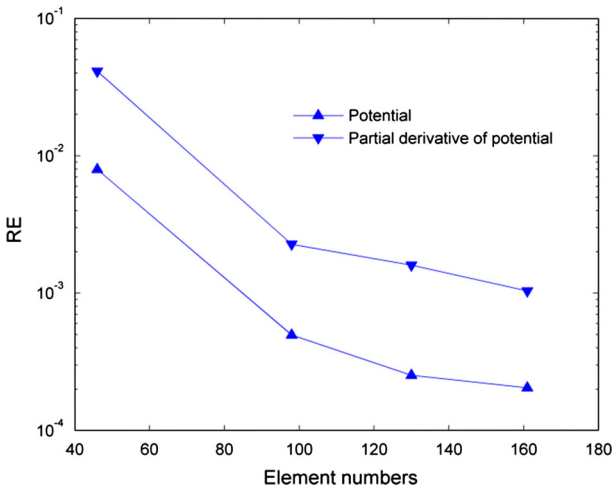

Fig. 6 Convergence curves of the potential and its derivative at interior point (3.999999, 0, 0)

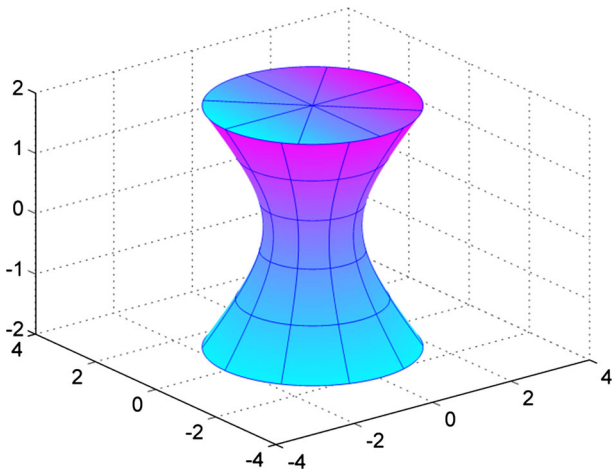

Fig. 7 A mixed boundary-value problem in a hyperbolic paraboloid

exact solutions which are also shown in Tables 1 and 2 and demonstrate the efficiency and the usefulness of the developed algorithm.

In addition, the convergence rates of the potential and its partial derivative, u and $\partial u/\partial x_1$, at the point (3.999999, 0, 0) are shown in Fig. 6, from which we can observe that the convergence rates of the computed potential u and its partial derivative $\partial u/\partial x_1$ are acceptable even when the distance between the computed point and the boundary reaches 10^{-6}.

Example 3 In this example, a mixed boundary-value problem with an oscillatory boundary condition is considered. The geometry of the problem is displayed in Fig. 7, and the parameter equation of the boundary can be given as:

$$x(\theta, t) = (\sqrt{1+t^2}\cos\theta, \quad \sqrt{1+t^2}\sin\theta, t), \quad \theta \in [0, 2\pi], \quad t \in [-2, 2].$$

On the boundary Γ, the potential u is prescribed on the top face and the bottom face, and the flux $q = \boldsymbol{n} \cdot \nabla u$ is given on the remaining surface components of Γ, where

$$u = e^{x_1}\cos\left(\frac{\sqrt{2}}{2}x_2\right)\cos\left(\frac{\sqrt{2}}{2}x_3\right),$$

$$\nabla u = e^{x_1}\left(\cos\left(\frac{\sqrt{2}}{2}x_2\right)\cos\left(\frac{\sqrt{2}}{2}x_3\right), -\frac{\sqrt{2}}{2}\sin\left(\frac{\sqrt{2}}{2}x_2\right)\cos\left(\frac{\sqrt{2}}{2}x_3\right), -\frac{\sqrt{2}}{2}\cos\left(\frac{\sqrt{2}}{2}x_2\right)\sin\left(\frac{\sqrt{2}}{2}x_3\right)\right).$$

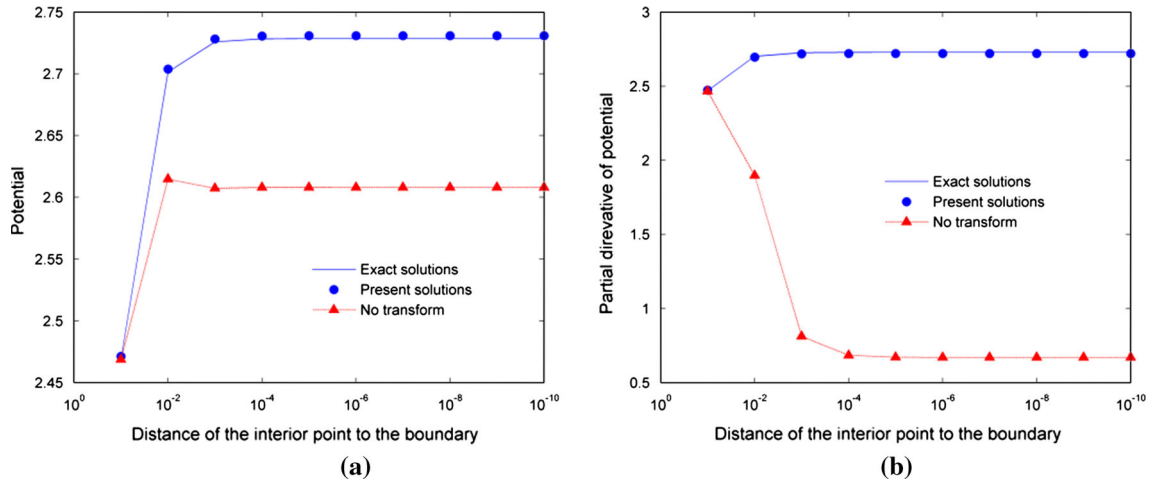

Fig. 8 Numerical results of the potentials (**a**) and its derivatives (**b**) at interior points close to the boundary

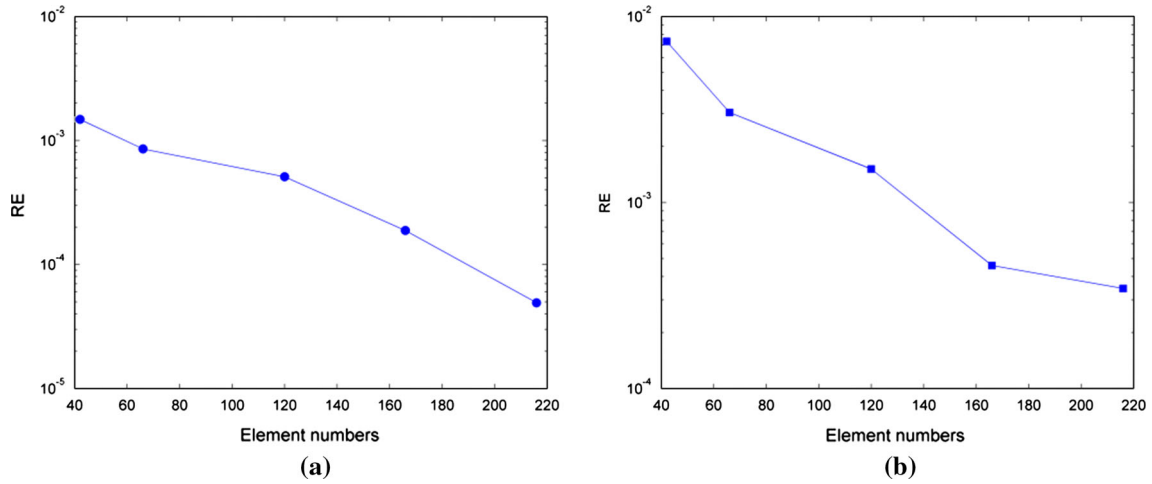

Fig. 9 Convergence curves of the potentials (**a**) and its derivatives (**b**) at an interior point

Sixty-six second-order quadrilateral surface elements are employed to depict the geometry boundary, in which 50 elements are on the side surface, 8 elements on the top surface and 8 elements on the bottom surface, respectively. Along the x_1-axis, Fig. 8 displays the numerical results of the potential and its partial derivative at inner points which are close to the boundary, respectively. From Fig. 8 we can observe that when the evaluation points are not too close to the integration element, the conventional method and the proposed method are both efficient, but the conventional method fails as the evaluation points are closer to the boundary. On the other hand, the results obtained by the proposed method are stable and satisfactory even when the distance of the evaluation point to the integration element is equal to 1.0E−9 or even smaller.

Besides, the convergence curves of the computed potentials u and its derivatives $\partial u/\partial x_1$ at a point, whose distance to the boundary equals 1.0E−6, are shown in Fig. 9; hence, we can observe that the convergence rates remain monotonic and rapid even when the distance from the field point to the boundary is as small as 1.0E−6.

Example 4 The computation of the nearly singular integral on a curved surface element is considered in this example [16]. The chosen surface element, named as spherical surface element [24], is represented in parametric form with the usual spherical polar system $(\theta,\ \varphi)$. And the element's geometric parameters are given as follows:$\theta \in [0,\ \pi/4]$, $\varphi \in [\pi/4,\ \pi/2]$, the sphere radius $r = 0.1$, and with center $(0, 0, 0)$. The projection point of the evaluation point is located at the center of the element. As given in Ref. [16], the relative distance between the evaluation point and the element is defined as $r_0/a^{1/2}$, where a stands for the element's area and r_0 is the minimum distance from the evaluation point to the element.

Table 5 Relative errors of various integrals with kernel u^* on a spherical surface element

$r_0/a^{1/2}$	10^{-1}	10^{-2}	10^{-3}	10^{-4}	10^{-5}	10^{-6}
Reference solution	0.0077988	0.0079031	0.0079136	0.0079147	0.0079148	0.0079148
Ref. [24] : (ρ, θ)	6.42E−9	2.52E−7	1.99E−6	6.09E−6	7.44E−6	9.11E−6
Ref. [24] : (α, β)	7.16E−9	2.52E−7	1.99E−6	6.09E−6	7.44E−6	9.11E−6
Present method	7.12E−9	2.47E−7	1.79E−6	5.06E−6	4.82E−6	4.53E−6

Table 6 Relative errors of various integrals with kernel q^* on a spherical surface element

$r_0/a^{1/2}$	10^{-1}	10^{-2}	10^{-3}	10^{-4}	10^{-5}	10^{-6}
Reference solution	0.2839962	0.2890126	0.2895177	0.2895683	0.2895733	0.2895783
Ref. [24] : (ρ, θ)	1.81E−7	4.48E−6	1.59E−6	7.89E−5	1.77E−4	1.50E−4
Ref. [24] : (α, β)	1.76E−7	4.48E−6	1.59E−6	7.89E−5	1.77E−4	1.50E−4
Present method	1.66E−7	4.12E−6	1.50E−6	7.69E−5	2.69E−4	2.14E−4

In Ref. [16], a new distance transformation is developed to remove the near singularity based on two local systems (ρ, θ) and (α, β). Tables 5 and 6 list the relative errors for the numerical evaluation of integrals with the kernels u^* and q^*, respectively, with the relative distance $d/a^{1/2}$ changing, using both the present method and the distance transformation. We can observe from the Table 5 and 6 that for these very simple test problems two methods can achieve very similar accuracies, and meanwhile, the relative errors for integrals with kernel u^* are both very small with the order less than 10^{-5}, whereas for integrals with kernel q^*, the relative errors reach 10^{-4}.

However, it should be pointed out that the distance transformation method in Ref. [16] possesses two major drawbacks: One is that when the four subtriangles, each of which is with projection point as one of its vertices, have unsuitable shapes depending on the position of the projection point, an adaptive element subdivision technique [24] is necessary to improve the computational accuracy. Such a procedure is sometime very cumbersome. The other drawback is that the distance transformation is not very effective for the evaluation of nearly hyper-singular integrals due to not fully eliminating their singularities. Compared with the distance transformation method in Ref. [16], the present method always works no matter where the position point is located. In addition, in the numerical implementation process of the present method, there is no need to define the aforementioned relative distance which is used here only for comparison purpose.

6 Conclusions

This study presents an improved scheme in order to numerically calculate 2D nearly singular integrals arising in 3D BEM. The scheme is an extension of the sinh transformation, which is used to evaluate the 1D or 2D nearly singular integrals on simple geometry elements, such as usual linear or planar elements, to 3D BEM using the eight-node second-order quadrilateral surface element. Three numerical examples with exact benchmark solutions are presented to test the proposed scheme, yielding very promising results. The results verify the feasibility and the effectiveness of the proposed scheme.

Acknowledgments The support from the Opening Fund of the State Key Laboratory of Structural Analysis for Industrial Equipment (GZ1307) and the National Natural Science Foundation of Shandong Province of China (ZR2010AZ003) is gratefully acknowledged.

References

1. Cerrolaza, M., Alarcon, E.: A bi-cubic transformation for the numerical evaluation of the Cauchy principal value integrals in boundary methods. Int. J. Numer. Meth. Eng. **28**, 987–999 (1989)
2. Scuderi, L.: A new smoothing strategy for computing nearly singular integrals in 3D Galerkin BEM. J. Comput. Appl. Math. **225**, 406–427 (2009)
3. Ye, W.J.: A new transformation technique for evaluating nearly singular integrals. Comput. Mech. **42**, 457–466 (2008)
4. Sladek, V., Sladek, J., Tanaka, M.: Optimal transformations of the integration variables in computation of singular integrals in BEM. Int. J. Numer. Methods Eng. **47**, 1263–1283 (2000)
5. Johnston, P.R.: Application of Sigmoidal transformations to weakly singular and near singular boundary element integrals. Int. J. Numer. Methods Eng. **45**, 1333–1348 (1999)

6. Johnston Barbara, M., Johnston, P.R., Elliott, D.: A new method for the numerical evaluation of nearly singular integrals on triangular elements in the 3D boundary element method. J. Comput. Appl. Math. **245**, 148–161 (2013)
7. Johnston, P.R., Elliott, D.: A sinh transformation for evaluating nearly singular boundary element integrals. Int. J. Numer. Methods Eng. **62**, 564–578 (2005)
8. Johnston, B.M., Johnston, P.R., Elliott, D.: A sinh transformation for evaluating two- dimensional nearly singular boundary element integrals. Int. J. Numer. Methods Eng. **69**, 1460–1479 (2007)
9. Elliott, D., Johnston, P.R.: The iterated sinh transformation. Int. J. Numer. Methods Eng. **75**, 43–57 (2008)
10. Johnston, P.R., Johnston, B.M., Elliott, D.: Using the iterated sinh transformation to evaluate two dimensional nearly singular boundary element integrals. Eng. Anal. Bound. Elem. **37**, 708–718 (2013)
11. Lv, J.H., Miao, Y., Gong, W.H. et al.: The sinh transformation for curved elements using the general distance function. Comput. Model. Eng. Sci. **93**, 113–131 (2013)
12. Lv, J.H., Miao, Y., Zhu, H.P.: The distance sinh transformation for the numerical evaluation of nearly singular integrals over curved surface elements. Comput. Mech. **53**, 359–367 (2014)
13. Huang, Q., Cruse, T.A.: Some notes on singular integral techniques in boundary element analysis. Int. J. Numer. Methods Eng. **36**, 2643–2659 (1993)
14. Ma, H., Kamiya, N.: Distance transformation for the numerical evaluation of near singular boundary integrals with various kernels in boundary element method. Eng. Anal. Bound. Elem. **26**, 329–339 (2002)
15. Ma, H., Kamiya, N.: A general algorithm for the numerical evaluation of nearly singular boundary integrals of various orders for two-and three-dimensional elasticity. Comput. Mech. **29**, 277–288 (2002)
16. Qin, X.Y., Zhang, J.M., Xie, G.Z. et al.: A general algorithm for the numerical evaluation of nearly singular integrals on 3D boundary element. J. Comput. Appl. Math. **235**, 4174–4186 (2011)
17. Miao, Y., Li, W., Lv, J.H., Zhu, H.P.: Distance transformation for the numerical evaluation of nearly singular integrals on triangular elements. Eng. Anal. Bound. Elem. **37**, 1311–1317 (2013)
18. Zhang, Y.M., Sun, C.L.: A general algorithm for the numerical evaluation of nearly singular boundary integrals in the equivalent non-singular BIEs with indirect unknowns. J. Chin. Inst. Eng. **31**, 437–447 (2008)
19. Zhang, Y.M., Gu, Y., Chen, J.T.: Boundary layer effect in BEM with high order geometry elements using transformation. Comput. Model. Eng. Sci. **45**, 227–247 (2009)
20. Zhang, Y.M., Gu, Y., Chen, J.T.: Internal stress analysis for single and multilayered coating systems using the boundary element method. Eng. Anal. Bound. Elem. **35**, 708–717 (2010)
21. Zhang, Y.M., Qu, W.Z., Chen, J.T.: BEM analysis of thin structures for thermoelastic problems. Eng. Anal. Bound. Elem. **37**, 441–452 (2013)
22. Xie, G.Z., Zhou, F.L., Zhang, J.M. et al.: New variable transformations for evaluating nearly singular integrals in 3D boundary element method. Eng. Anal. Bound. Elem. **37**, 1169–1178 (2013)
23. Zhang, Y.M., Li, X.C., Sladek, V., Sladek, J., Gao, X.W.: Computation of nearly singular integrals in 3D BEM. Eng. Anal. Bound. Elem. **48**, 32–42 (2014)
24. Qin, X.Y., Zhang, J.M., Xie, G.X. et al.: A general algorithm for the numerical evaluation of nearly singular integrals on 3D boundary element. J. Comput. Appl. Math. **235**, 4174–4186 (2011)